How Shape Influences Uptake: Interactions of Anisotropic Polymer Nanoparticles and Human Mesenchymal Stem Cells

Laura Florez, Christine Herrmann, Jens M. Cramer, Christoph P. Hauser, Kaloian Koynov, Katharina Landfester, Daniel Crespy, and Volker Mailänder*

Among several nanoparticle properties, shape is important for their interaction with cells and, therefore, relevant for uptake studies and applications. In order to further investigate such characteristics, fluorescently labeled spherical polymer nanoparticles are synthesized by free-radical polymerization via the miniemulsion process. The spherical nanoparticles are subsequently submitted to controlled mechanical deformation to yield quasi-ellipsoidal polymeric nanoparticles with different aspect ratios. The uptake behaviors of spherical and non-spherical particles with equal volume are investigated qualitatively and quantitatively by electron microscopy, confocal laser scanning microscopy, and flow cytometry measurements. Non-spherical particles show fewer uptake by cells than their spherical counterparts with a negative correlation between aspect ratio and uptake rate. This is attributed to the larger average curvature radius of adsorbed non-spherical particles experienced by the cells.

1. Introduction

Current intensification of research on particle–cell interactions led scientists to consider parameters other than the "traditional" ones, which are the surface chemistry and the size of particles.[1–3] For example, the softness and hydrophobicity of the nanomaterials used for cellular uptake studies is a parameter that was investigated in recent years.[4] The shape of particles was also found to play a crucial role for uptake in cells,[5–8] and was instituted as a new important parameter for designing materials able to induce a specific biological response.[9] Ferrari and colleagues predicted[10] and demonstrated[11] the importance of the shape on the adhesion of particles on cell layers and their biodistribution in tumor-bearing mice.

In contrast to inorganic anisometric materials which are relatively easy to synthesize, man-made polymeric anisotropic particles are seldom reported in the literature. The physical methods employed to synthesize non-spherical nanoparticles are soft lithography,[12–15] microfluidics,[16] or techniques based on the mechanical deformation of spherical particles or droplets (stretching, compressing, shearing).[17–25] The methods based on the modification of pre-existing particles are particularly interesting since they allow the fabrication of polymer nanomaterials with functionalized surfaces, e.g., different charges, selective ligands, and receptors. Functionalized particles can be embedded in a hydrophilic[17] or hydrophobic[23] polymer matrix and the composite film is subsequently submitted to mechanical deformation at temperatures above the T_g of both polymers and then cooled. One additional advantage of the stretching method is that nanoparticles with

L. Florez,[+] C. Herrmann,[+] J. M. Cramer,
Dr. C. P. Hauser, Dr. K. Koynov, Prof. K. Landfester,
Dr. D. Crespy, Dr. V. Mailänder
Max Planck Institute for Polymer Research
Ackermannweg 10, 55128 Mainz, Germany
E-mail: crespy@mpip-mainz.mpg.de
Dr. V. Mailänder
III. Medical Clinic (Hematology, Oncology and Pulmonology)
University Medicine of the Johannes-Gutenberg University
Mainz, Langenbeckstrasse 1, 55131 Mainz Germany
[+] Both authors contributed equally.

DOI: 10.1002/smll.201102002

small NANO MICRO

capsular morphologies can be also deformed mechanically;[22] whereas no anisometric nanocapsule morphology has yet been reported with lithographic methods.

Ideal material candidates to be stretched for nanoparticle–cell interaction should allow facile tuning of their size and chemistry. Miniemulsion polymerization was already found to be a suitable technique to produce polymer nanoparticles with a predictable size-range and chemistry.[26] The latexes fabricated with the miniemulsion process were used for nanoparticle–cell studies[1] and were recently proposed as candidates for the immobilization of metallo- and prodrugs.[27] Efficient encapsulation of either hydrophobic[28–31] or hydrophilic[32–34] agents was also demonstrated using miniemulsion droplets as templates.

There are, to date, few general answers to fundamental questions related to the toxicity and interactions of nanoparticles with cells. Studies reported in the literature mainly deliver only specific answers since the nanoparticles are either insufficiently characterized and/or the biological investigations do not follow a universal protocol. The nanoparticles must be characterized after every manipulation because their composition and cellular uptake can be altered even by very low amounts of components, especially if they are present on the surface of the nanoparticles.[35] The immediate consequence is that non-empirical modeling is difficult to compare with experimental data. We aim here at comparing well-characterized functionalized spherical and non-spherical model colloids. Such model colloids were created through a combination of miniemulsion polymerization and an optimized stretching process. The uptake of the obtained non-spherical nanoparticles by human mesenchymal stromal and HeLa cells (a cell line established in 1951 and derived from cervical cancer cells taken from the patient Henrietta Lacks) was investigated via qualitative and quantitative measurements. To assess the generality of the conclusions, the experiments were performed with two different human cell-types. Mesenchymal stem cells (MSC) have been selected as they are primary cells of the human organism. They show high proliferation and differential potential and are highly interesting candidates for regenerative medicine. HeLa cells were chosen as cellular model for malignant cells.

2. Results

2.1. Synthesis of Fluorescent-Labeled Spherical Nanoparticles

The fluorescent dyes *N*-(2,6-diisopropylphenyl)-perylene-3,4-dicarboximide (PMI) and B504-MA (copolymerizable derivate of a boron dipyrromethene dye; Figure S1 of the Supporting Information (SI)) were encapsulated in the nanoparticles. Prior experiments following the procedure reported by Ho et al.[17] yielded very low solid content of dispersions after the removal of polyvinyl alcohol (PVA) and showed the formation of aggregates (see nanoparticles NP_1 , Table S1 in the SI). First experiments for studying their interaction with cells showed that aggregates of particles were already present at the surface of the cells (Figure S2, SI) and, therefore, they were not further discussed in the present document. This was attributed to the loss of surfactant in the repeated washing/centrifugation process. To circumvent the problem it was possible to copolymerize the main monomer (here styrene) with a hydrophilic co-monomer which ensures electrostatic stabilization even after the washing cycles.[22] Some authors using the stretching method reported that the latexes employed for the study were functionalized with sulfate groups.[17,20,21] We introduced sulfonate groups (not sulfate) via the copolymerization of styrene with a sulfonate-functionalized monomer (SSNa), which yielded a high density of charges on the particles NP_2. The particles were still electrostatically stabilized even without the surfactant sodium dodecyl sulfate (SDS), i.e., after the washing and centrifugation procedures. The number of charges per nm^2 on the particle surface was quantified to be 0.9 groups/nm^2 (dialyzed sample, **Table 1**). This is more than the charge density reported for polystyrene functionalized with aminoethylmethacrylate hydrochloride (0.2 groups/nm^2 at pH = 4.0), and lower than the charge of particles functionalized with acrylic acid (2.7 groups/nm^2 at pH = 9.0) for the same weight percent (wt%) amount of co-monomer.[36] However, it is more appropriate to compare the groups/nm^2 with similar mole percent (mol%) of co-monomer in the copolymerization feed. In this case, the copolymerization with SSNa yields about the same charge density compared with acrylic acid (1.2 groups/nm^2). 33 wt% of the styrene sulfonate (0.9 wt% compared to the total amount of polymer) was not polymerized as measured by ^{1}H-NMR spectroscopy (Figure S3, SI). This represents only a low amount of unbound styrene sulfonate for the nanoparticles diluted for cell experiments NP_2 (<0.25 wt%) and hence even lower for the thermally treated, but non-stretched, nanoparticles (i.e., NP_2+*T*-*S*), and the thermally treated and stretched nanoparticles (i.e., NP_2+*T*+*S*). This is important to note since sulfonate ions have very good salting-out properties in the Hofmeister series. The copolymerization of styrene and styrene sulfonate in miniemulsion was successful as measured by gel permeation chromatography (GPC) (M_n ~ 66 000 g mol^{-1}, see Table 1). See Experimental Section for further information about the annotations NP_i+*T*±*S*.

Table 1. Characteristics of the dispersion and polymer used in this study.

Entry	D_h[a] [nm]	D[b] [nm]	Groups/nm^2	M_n [g mol^{-1}]	M_w [g mol^{-1}]
NP_2	127 ± 18	100 ± 15	0.9	66 000	222 000

[a]Measured by DLS; [b]Measured by SEM.

2.2. Synthesis and Characterization of Quasi-ellipsoid Nanoparticles

We successfully prepared stretched nanoparticles and their shapes are denominated as quasi-ellipsoids. In fact, the stretched particles do not present an ellipsoidal shape at higher draw ratio (**Figure 1**d). The perimeter of the cross-sections of such ellipsoids cannot be described with an ellipse function.

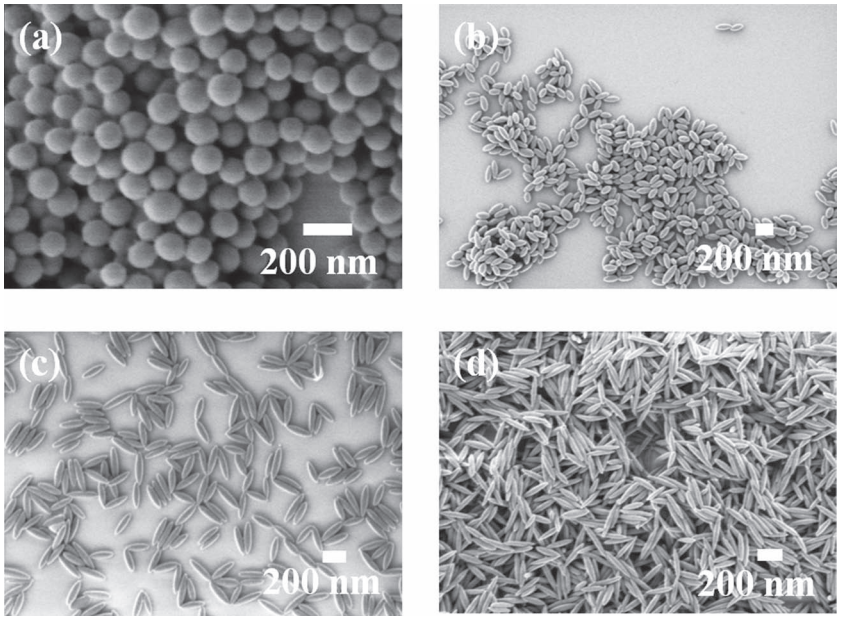

Figure 1. SEM micrographs of: a) NP_2+T-S_0; b) NP_2+T+S_{50}; c) NP_2+T+S_{100}; d) NP_2+T+S_{150}.

The main drawback of the stretching method is that it is normally not possible to remove all the polymer material, which was used as matrix for dispersing the nanoparticles to be stretched. The presence of this polymer layer around the elongated nanoparticles has a direct influence on colloidal properties such as stability and size. Because nanoparticle surface properties play an important role for uptake in cells,[1,3] it is necessary to determine the differences between the synthesized nanoparticles NP_i, NP_i+T+S (nanoparticles with temperature treatment and stretching) and NP_i+T-S (nanoparticles with temperature treatment and without stretching) and to verify that they cannot have an influence on the particle-uptake. When a variable was identified as a potential significant contributor to the extent of nanoparticle uptake by cells, additional cell uptake experiments were done.

Apart from the obvious difference in shape imparted by the stretching process, there are also differences due to the process itself. One of them is the presence of a PVA layer or the absence of SDS after the washing on the nanoparticles when comparing NP_i with the other nanoparticles (especially temperature-treated nanoparticles without stretching NP_i+T-S) as discussed above. A second difference between the nanoparticles NP_i and NP_i+T-S or NP_i+T+S is the presence of isopropanol during the washing process. The residual amount of isopropanol in the dispersion was measured to be 0.14 wt% by ^{1}H-NMR spectroscopy, which means concentrations as low as 0.2 and 0.4 wt% in the cell media with 75 μg mL^{-1} and 150 μg mL^{-1}, respectively. Isopropanol has therefore no influence on the uptake studies. A speculative orientation of polymer chains (and, therefore, birefringence) expected in the quasi-ellipsoids is not considered as an important parameter that can influence the particle uptake. We also verified by FT-IR and NMR spectroscopy that the sulfonate groups did not react with the hydroxyl group of PVA to yield a sulfonic acid ester.

Although it may influence considerably the surface property of the particles, their stability, and ultimately the uptake of nanoparticles in cells, the PVA layer is seldom measured or characterized. To the best of our knowledge, only one article reported semi-quantitative measurement of residual PVA on particles after the stretching and washing processes.[37] The authors compared the diameter of non-stretched spherical polystyrene particles without and with treatment (NP_i and NP_i+T-S in our notation). They measured a difference of 10 nm by electron microscopy for particles having diameters around 200 nm. The same group compared the electrophoretic mobility of both particles and found that particles of the NP_i+T-S type displayed lower mobility, which was attributed to the presence of residual PVA as a shell.[38] Another group compared the zeta potential of particles of type NP_i (–53 mV) with particles of type NP_i+T-S (–57 mV).[20] No quantitative information about the PVA shell thickness was extracted from such measurements. We tried without success to titrate polyvinyl alcohol via spectroscopic methods reported in the literature.[39] The amount of PVA was also not detectable by ^{1}H-NMR measurements on polymers from purified, stretched particles dissolved in DMSO-d_6. The PVA was probably too strongly adsorbed on the particles and it was not possible to detect the PVA even after treatment of the particles with acids, bases, temperature, or sonication.

Therefore, we estimated the size of the PVA layer by zeta potential measurements assuming that the thickness of the PVA layer was proportional to the logarithm of the zeta potential for a flat double layer (see Equation 1).[40] The fact that the adsorption of PVA on negatively charged nanoparticles leads to a shielding of the charges led us to estimate the PVA amount on the nanoparticles by zeta potential measurements. Different amounts of PVA were added to the original dispersion NP_2 and the zeta potential of the obtained latexes was recorded (see Figure S4, SI) and compared to the zeta potential of sample NP_2+T-S (–44 mV). Additional DLS experiments showed that the mean diameter of the particles increased if PVA was added, which is explained by the adsorption of PVA on the particle surface (Table S2, SI). No bimodal or multimodal distribution was observed. This fact combined to the only slight increase of diameter of the particle implies that no coagulation took place due to the addition of PVA. With the assumptions previously described,[40] the zeta potential ζ can be expressed as:

$$\zeta = \Psi_d \cdot \exp\left[-\kappa(\delta - \Delta)\right] \quad (1)$$

with Ψ_d, κ, δ, Δ being the Stern potential, the reciprocal of the Debye–Hückel length, the thickness of the adsorbed polymer

NANO MICRO small

Table 2. Characteristics of the nanoparticles.

Entry	Draw ratio [%]	Diameter[a] [nm]		Aspect ratio
NP_2+T-S_0	0	100 ± 15,[a] 127 ± 18[b]		1
		Polar axis[a] [nm]	Equatorial axis[a] [nm]	
NP_2+T+S_{50}	50	191 ± 23	84 ± 9	2.3
NP_2+T+S_{100}	100	279 ± 30	70 ± 8	4.0
NP_2+T+S_{150}	150	381 ± 47	65 ± 7	5.9

[a]Measured by SEM; [b]Measured by DLS.

layer, and the thickness of the Stern layer, respectively. The thickness of the PVA layer was found to be 1 nm according to Equation 2:

$$d = \frac{D}{2} \cdot \left[\sqrt[3]{\left(1 + \frac{\rho_{PS} \cdot m_{PVA}}{\rho_{PVA} \cdot m_{PS}}\right)} - 1 \right] \quad (2)$$

and approximating the density of the polystyrene and PVA in our system with the density of the polymers in bulk, i.e., 1.04 and 1.27 g cm^{-3}, respectively. The approximation is incorrect because we expect the density of the PVA layer to be much higher since PVA swells in water. The difference between the average diameter of NP_2+T-S and NP_2 was 5 and 10 nm as measured by SEM and DLS, respectively. A correct estimation given by zeta potential measurements is the amount of PVA compared to the total amount of polymers (PVA+PS), which is 7.3 wt%.

In order to investigate the influence of the aspect ratios on the uptake rate into cells we used 50, 100, and 150% draw ratios for stretching (see **Table 2** and Figure 1). The nanoparticles were assumed to be spheroids (2 equal half-axes) after stretching and, therefore, we approximate their shape as a prolate shape. As the PMI dye which was used in the first experiments as fluorescent label in the nanoparticles is only physically absorbed we also evaluated the nanoparticles with the covalently bound dye B504-MA and determined their concentration and fluorescence brightness by fluorescence correlation spectroscopy (FCS). The brightness of the nanoparticles was found to remain unchanged after the thermal treatment and the extensive washing steps, as measured by FCS and with the plate reader monochromator. This was true for physically absorbed fluorescent dye PMI and for the covalently bound dye B504-MA.

2.3. Qualitative Assessment for the Influence of the Shape on Particle-Uptake in Cells

For quantitative uptake studies aggregation and strong adhesion to cell surfaces without uptake is a major disadvantage and should be avoided wherever possible. Therefore, confocal laser scanning microscopy (cLSM) measurements were performed. These showed that the particles were internalized in MSCs and HeLa cells with little co-localization to the cell surface (**Figure 2**).

Furthermore SEM and TEM microscopy were carried out to investigate the location and orientation of the nanoparticles

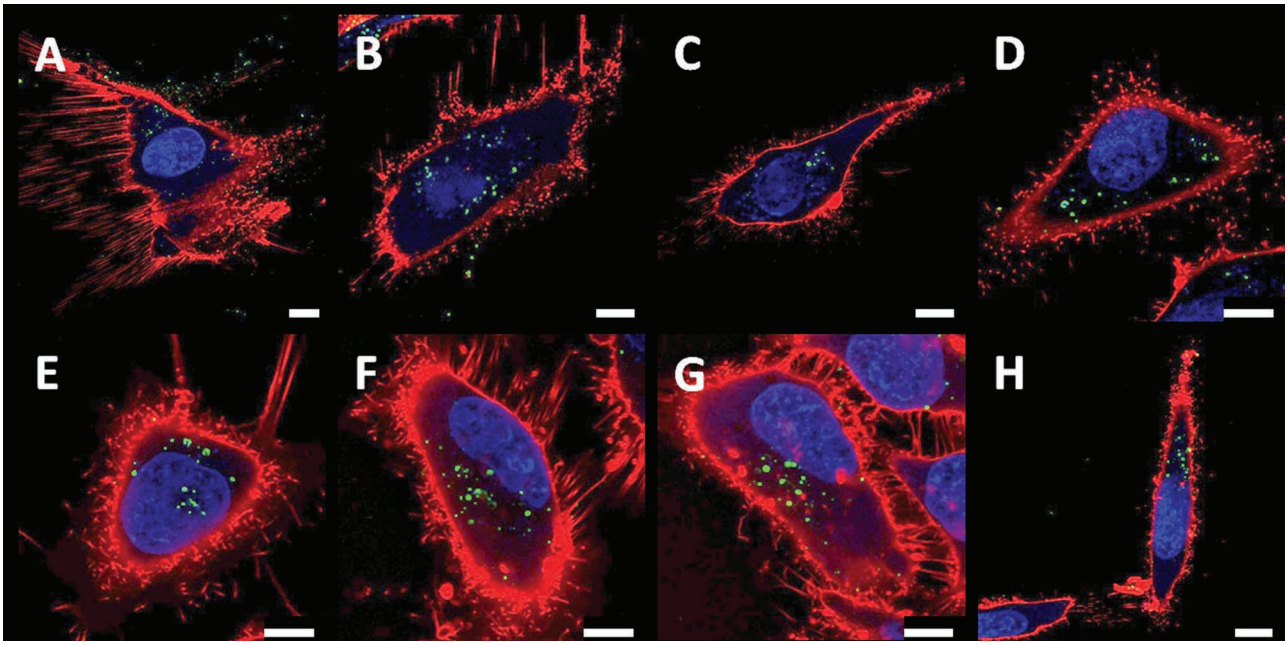

Figure 2. Uptake of spherical and ellipsoidal nanoparticles into MSC- (A–D) and HeLa-cells (E–H) after 20 h of incubation at a concentration of 75 µg mL^{-1} added to the cell culture medium. The particles with B504-MA are pseudocolored in green, the cell membrane is shown in red (CellMaskOrange Plasma Stain), and the cell nuclei are pseudocolored in blue (DraQ5). A,E) NP_2; B,F) NP_2+T+S_{50}; C,G) NP_2+T+S_{100}; D,H) NP_2+T+S_{150}. The scale represents 10 µm.

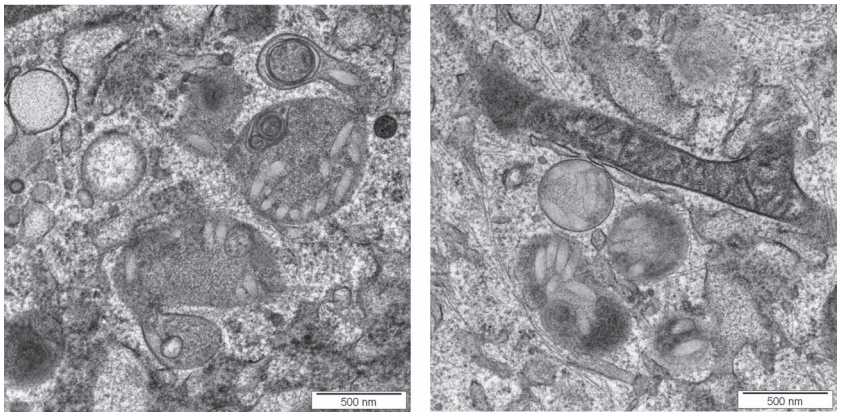

Figure 3. TEM micrographs of particles of type NP_2+T+S_{100} internalized in MSCs after 20 h (150 µg mL^{-1}).

at the cell membrane and in the cell, respectively. Spherical as well as quasi-ellipsoids could be detected as single particles and as aggregates of particles on the cell membrane (Figure S5 for ellipsoidal and Figure S6 for spherical nanoparticles, see SI). The stretched nanoparticles were always seen lying flat on the cell membrane. Some cells were accidently damaged through one of the preparation procedures; therefore, intracellularly located nanoparticles could be detected in this SEM study (Figure S6c,d of the SI). The ellipsoidal nanoparticles were detected to be partly arranged side-by-side and partly packed in, what was suspected to be endosomal compartments. TEM studies showed that ellipses and circles (depending if the sample was cut along the equatorial or polar axis of the quasi-ellipsoid during the preparation) were observed in intracellular compartments (**Figure 3**), confirming that the stretched nanoparticles were efficiently internalized.

2.4. Cell Experiments: Cell Vitality

A further prerequisite is that the nanoparticles are non-toxic. Cell vitality was evaluated after particle addition to MSCs as a more sensitive, primary cell type compared to malignant cell lines like HeLa cells for different uptake times (1, 20, and 48 h) as well as different particle concentrations (9.4; 18.8; 37.5; 75; 150, and 300 µg mL^{-1}). None of the particles (spherical not treated, spherical treated, ellipsoid treated at any stretch rate) were toxic at any of the tested conditions. In every case at least 98% of the gated cells were still alive and no significant differences were identified among the evaluated conditions for the three different particle types (Figure S7 and Figure S8, SI).

2.5. Influence of the Embedding and Recovery Procedure on Nanoparticle-Uptake

An accurate determination of the cell-uptake in cells by fluorescence activated cell sorter (FACS) can only be performed if the fluorescence brightness of the different particles to be compared is measured prior to the measurements. Indeed, the preparation method of stretched nanoparticles can lead to bleaching of some dyes. For this, a double check was carried out to calibrate the FACS measurements with the fluorescence brightness of the nanoparticles as measured by FCS and plate reader techniques. No significant differences were found when the calibration was realized by one or the other technique.

Embedding and recovery of the nanoparticles from the PVA film may alter many components and composition of the nanoparticles as detailed above. Therefore we investigated if this would influence the uptake into cells. Indeed, we found consistently in multiple experiments (n = 2, n′ = 4)[41] that embedded and recovered spherical nanoparticles NP_2+T-S were taken up at a higher rate than the original nanoparticles (NP_2, see **Figure 4**).

One of the factors which has been determined to differ between the NP_i and the NP_i+T-S is the amount of styrene sulfonate sodium (SSNa) as the recovery procedure reduces the amount of SSNa. We therefore added SSNa before incubation in cell culture with the NP_i+T-S nanoparticles. No difference in uptake efficiency was determined for the addition of SSNa (Figure S9, SI)

Another difference is the presence of PVA in the dispersion. We added PVA at different concentrations and showed that the addition of PVA reduces uptake (Figure S10, SI), thereby contradicting the hypothesis that NP_i+T-S (which should have a PVA coat) versus NP_i should be taken up in larger amount.

2.6. Nanoparticle Concentration and Uptake Maximum of Non-stretched (NP_i+T-S) Versus Stretched Nanoparticles (NP_i+T+S_{100})

A study on the influence of particle concentration on uptake was performed with an increasing amount of nanoparticles

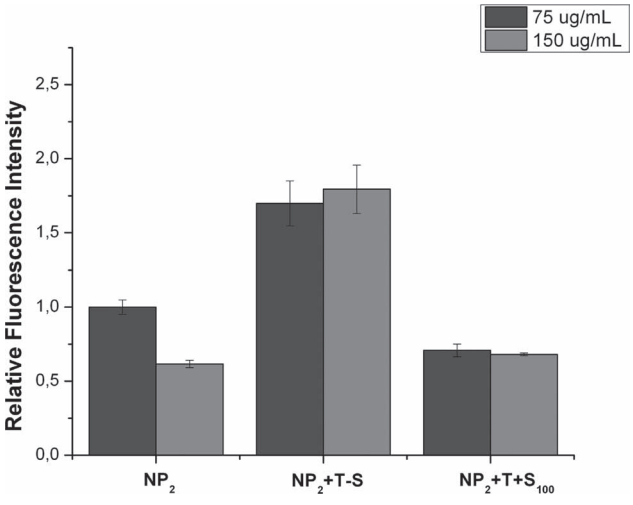

Figure 4. Investigations of NP_2- and (NP_2+T-S)-uptake by flow cytometry after incubation in MSC after 20 h.

small NANO MICRO

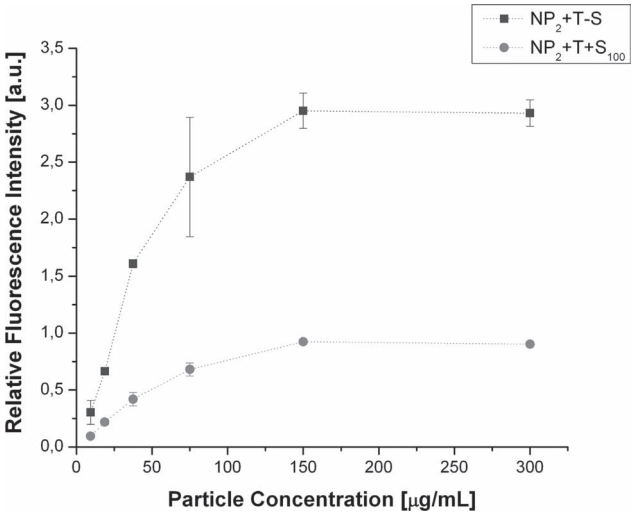

Figure 5. Quantitative assessment of the influence of the nanoparticle concentration for NP_2+T-S and NP_2+T+S_{100} on particle-uptake in MSC after 20 h incubation.

using NP_2+T-S and NP_2+T+S_{100} . As can be seen in **Figure 5**, the stretched nanoparticles (NP_2+T+S_{100}) showed less uptake compared to non-stretched particles (NP_2+T-S) at all concentrations. Since the amount of all nanoparticles that have been embedded and recovered was limited, 75 μg mL^{-1} was chosen as a compromise between maximum uptake (which would have been favored by the 150 μg mL^{-1} concentration) versus lower concentrations where the fluorescence signal was lower.

We also investigated how long we needed to incubate the unstretched NP_2+T-S versus stretched nanoparticles NP_2+T+S_{100}. Here we observed that no saturation was reached for the incubation times chosen (see Figure S11 of the SI), but because the signal is sufficiently strong after 20 h we chose this as the standard incubation time.

2.7. Influence of Aspect Ratio on Nanoparticle-Uptake

While all previous results have been obtained with non-stretched NP_2+T-S versus stretched nanoparticles NP_2+T+S_{100} we varied the draw ratio of the films and, therefore, the aspect ratio of the nanoparticles. The uptake of anisotropic nanoparticles NP_2+T-S was compared to NP_2+T+S_{50}, NP_2+T+S_{100}, and NP_2+T+S_{150}. NP_2+T+S_{150}, which are taken up by MSC (**Figure 6**a) and HeLa cells (Figure 6b) to a considerably lesser extent.

3. Discussion

The results are particularly interesting since they add relevant information on recent findings dealing with interactions between anisotropic particles and cells. Chithrani et al.[5] prepared polydisperse gold nanoparticles with different sizes and shapes. A total absence of cetyltrimethylammonium bromide (surfactant) introduced by the chemical process to fabricate

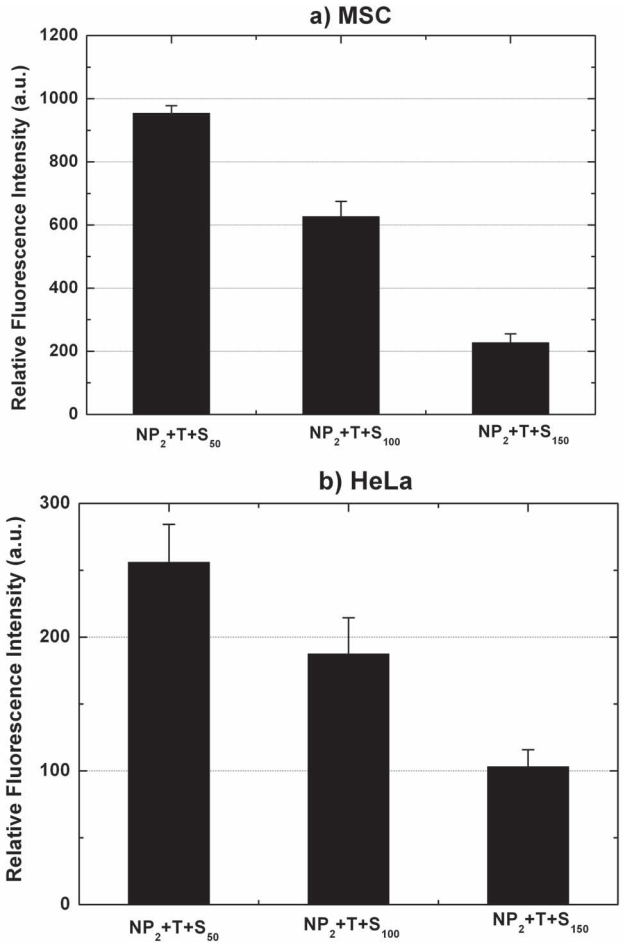

Figure 6. Uptake of nanoparticles with different aspect ratios in: a) MSC, and b) HeLa cells.

the rod nanoparticles could not be proven. Since the spherical nanoparticles were only stabilized by citric acid, the surface chemistry of both kinds of particles was different. The second fact is that the compared spherical and rod-like nanoparticles did not have the same volume and, therefore, the constant in the experiments was the average value of the width and the height of the rods. The results tend to show that nanoparticles with higher aspect ratio showed less uptake by HeLa cells. The uptake was found to decrease in the following order: spherical nanoparticles > nanorods with aspect ratio of 3 > nanorods with aspect ratio of 5. These results are in line with our observations (Figure 6). Arnida et al. showed that gold nanorods were taken up less efficiently by the macrophage cell line than gold nanoparticles, as monitored by inductively coupled plasma mass spectrometry (ICP-MS).[42] Qiu et al. investigated the uptake and cytotoxicity of gold nanorods coated with a cationic surfactant, a polyanion, or a polycation.[43] In all cases, the uptake by MCF-7 cells of nanorods with an aspect ratio of 4 was less favored compared to nanorods with an aspect ratio of 1.1. In both cases,[42,43] the compared nanoparticles had a different volume.

Gratton et al. synthesized nanoparticles of different shapes with a mixture of crosslinker (main component), polymerizable oligo(ethylene glycol), hydrophilic

amino-functionalized monomer, polymerizable dye, a photoinitiator, and 2-propanol as solvent.[7] Since it is not proven that there is no spatial deviation of composition for the nanoparticles obtained (substrate is crosslinked Fluorocur), it is not clear what surface material the cells really experience when they come in contact. The zeta potential of the particles was also estimated to be different depending on their sizes and geometry (not kept constant). The kinetics of internalization is four times larger for cylindrical particles with aspect ratio of 3 (~450 nm × 150 nm) than for cylindrical particles with aspect ratio of 1 (200 nm as diameter and height). The authors did not a find clear explanation for this behavior.

Meng et al. synthesized mesoporous silica nanoparticles with different aspect ratios (1.5, 2.1, 4.0) and different volume and investigated their uptake in cells.[44] The rod-like nanoparticles originally displayed a positively charged surface before being dispersed in cell medium. The highest uptake was found for nanoparticles with an aspect ratio of 2.1, whereas nanoparticles with an aspect ratio of 4.0 displayed the lowest uptake rate. This observation is in line with our results. Meng et al. also demonstrated that macropinocytosis is involved in the uptake of the particles. Our work also demonstrates that polymeric nanoparticles can be as versatile as their inorganic counterparts for the investigations concerning the aspect ratio of the particles. The advantage of the present method is that the investigations are performed with exactly the same polymer materials. Other methods for obtaining nanoparticles with different aspect ratios involve the need for one batch per synthesis.

A number of considerations have to be taken into account to analyze the results. At constant volume, the average coefficient of diffusion of prolate ellipsoids is higher than spheres. This means that the prolate will meet the cell membrane earlier than the spheres do. However, this fact does not influence the amplitude of uptake in cells because the FACS measurements include concentrations at which the plateau where cells are saturated with nanoparticles has been reached.

Herein we try to give a mechanistic understanding for the observed phenomena and to identify the factors that influence the uptake. We propose to explain the decrease of the nanoparticle uptake with increasing aspect ratio by the fact that the cells need to wrap around the poles (i.e., along the polar axis) during the uptake procedure. The orientation of the nanoparticles after adsorption on the cells and the density of functional groups are therefore important. Indeed the mean curvature radii of the nanoparticles used in this study are not significantly different from each other (see calculation and Table S3 in the SI), i.e., 50, 54, 50, and 48 for NP_2+T-S_0, NP_2+T+S_{50}, NP_2+T+S_{100}, and NP_2+T+S_{150}, respectively.

Therefore, we compared the surface of the poles of the prolate and the total surface of the ellipsoid (see Figure S12 of the SI). For the sake of simplicity, the surface of the poles are maximized by the surface of two hemispheres with radius $b/2$, i.e., $A_{p} < A_{p'} = 2\pi b^2$. With $\gamma = a/b$, where a = polar axis, we obtain:

$$\frac{A_{\text{prolate}}}{A_{p'}} = 1 + \gamma \cdot \frac{\arcsin\sqrt{1-\gamma^{-2}}}{\sqrt{1-\gamma^{-2}}} \quad (3)$$

The inverse gives the relative importance of the surface of the poles compared to the total surface of the ellipsoids and was found to be 26, 16, and 11% for the particles stretched at 50, 100, and 150% draw ratio, respectively. This explains why the stretched nanoparticles adsorb preferentially along the polar axis on cell membranes as observed via SEM measurements (Figure S5 of the SI).

The direct consequence is that cells detect objects with very low curvature if compared to the curvature of spherical nanoparticles $2/D$, where D = diameter of the sphere. Adsorbed stretched nanoparticles behave as spherical particles with an equivalent apparent curvature. The maximal curvature radius for an ellipse with coordinates a,b is a^2/b, hence yielding maximal curvature radius of 217, 556, and 1120 nm for the samples NP_2+T+S_{50}, NP_2+T+S_{100}, and NP_2+T+S_{150} respectively, compared to the 50 nm of the spherical non-stretched nanoparticles NP_2. It has been shown that macropinocytosis, clathrin-mediated and caveolin-mediated endocytosis are strongly size-dependent since the endocytotic vesicles have an upper size limit.[45] Hence, as the nanoparticles appear (for the cells) to be very large, specific uptake mechanisms might be constrained.

Another effect that may reinforce preferential adsorption of ellipsoids on cells along their polar axis is that in principle the surface density of charges is no longer constant after stretching. Assuming that there is no re-distribution of the functional groups during the stretching process, the distribution of charge over the surface of an elongated particle starting from isotropic spherical particles can be expressed as:

$$\sigma_{\text{prolate}} = \frac{\sigma_{\text{sphere}} \cdot \lambda}{\sqrt{\cos^2\theta + \lambda^3 \cdot \sin^2\theta}} \quad (4)$$

The charge distribution for the three nanoparticles NP_2+T+S_{50}, NP_2+T+S_{100}, and NP_2+T+S_{150} is plotted in Figure S13 of the SI. This effect may be buffered by the presence of the PVA shell. Indeed Ho et al. were not able to demonstrate a dependence of the adsorption of smaller spherical nanoparticles on large prolate microparticles on the azimuthal angle in heterocoagulation experiments.[46] Because the cell surface is negatively charged (1.2×10^{-2} electrons per nm^2 for HeLa cells),[47] Coulombic interactions will favor the adsorption of negatively charged ellipsoids along the polar axis, and not on their edge, where there is a high density of negative charges. Finally, it is worth mentioning that although the HeLa and MSC cells differ in many aspects (cell division and cell differentiation), the trend of lesser uptake by ellipsoids was confirmed for both cell types.

4. Conclusion

Fluorescent prolate nanoparticles with different aspect ratios were prepared by stretching spherical nanoparticles synthesized by miniemulsion polymerization. Subsequently, their interactions with MSC and HeLa cells were investigated. A clear correlation between increase of aspect ratio and decrease of uptake was observed and was independent of the cell type. We consider that the aspect ratio alone cannot be chosen as

NANO MICRO small

sole parameter to explain this trend. In addition, we propose that the preferential adsorption of ellipsoid nanoparticles along their polar axis leads the cells to experience materials with reduced curvature than their counterparts with lower aspect ratio. Thus, both chemistry and shape are crucial factors for predicting the uptake of nanoparticles in cells.

This finding suggests that elongated shape-changing nanoparticles functionalized with specific ligands would be suitable drug-delivery vehicles. Indeed, the selectivity would be increased because the surface offered by the elongated particles is higher than the surface of spherical particles. The shape-changing effect shall ensure retrieval of the original spherical shape upon external stimuli for highest uptake in cells once the targeted cells are found by the particles.

5. Experimental Section

Materials: The synthesis of the fluorescent dye B504-MA was reported in the literature,[48] and the structure is displayed in Figure S1 of the SI. Demineralized water was used throughout the work. The purity and origin of the other chemicals are detailed in the SI.

Synthesis of the Spherical Functionalized Nanoparticles: The nanoparticles were synthesized based on the procedure reported earlier.[22,49] The nanoparticles are labeled NP_i in the text and the composition is given in **Table 3**.

Stretching of the Film and Particle Recovery: The stretching and recovery of the nanoparticles described below follows a modified version of the experimental procedure that was originally described by Ho et al.,[17] and that is detailed in the SI.

Analytical Methods: The dynamic light scattering, fluorescence correlation spectroscopy, zeta potential, and particle charge detector measurements of the dispersions and their dialysis are described in the SI. Further specifications regarding the autocorrelation function employed are described in the literature.[50] The polymers were analyzed by UV-vis spectroscopy, DSC, and GPC; and the particles were analyzed by electron microscopy. The remaining styrene sulfonate and isopropanol were quantified by ^{1}H-NMR (see SI).

Analytical Methods Cell Culture: MSCs were provided by collaborators in the Institute of Clinical Transfusion Medicine and Immunogenetics at the University of Ulm, Germany. The cells were generated from bone marrow aspirations or explanted hips, as described before,[36] after obtaining informed, signed consent. Cell differentiation and presence of surface markers were determined as published previously,[51] and MSCs were kept in α-MEM (minimum essential medium, Lonza, Switzerland) supplemented with 20% fetal bovine serum, 1% penicillin/streptomycin, 1% sodium pyruvate, and ciprofloxacin (2 mg mL^{-1}). HeLa cells were kept in DMEM (Dulbecco's modified Eagle's medium) supplemented with 100 U penicillin, 100 µg mL^{-1} streptomycin and 10 vol% fetal calf serum. Cells were grown in a humidified incubator at 37 °C and 5% CO_2. Cell seeding and preparation protocols varied according to the specific analysis method as described in the SI. The details about the experimental procedures of flow cytometry, confocal laser scanning microcopy, and electron microscopy performed on the cells are given in the SI.

Table 3. Composition of the miniemulsion used for the synthesis of sulfonated polystyrene fluorescent particles NP_2.

Component	Function	Weight [g]
V59 [2,2′-azobis-(2-methylbutyronitrile)]	oil-soluble initiator	0.10
styrene	monomer	5.82
hexadecane	hydrophobic stabilizing agent	0.26
SDS	anionic surfactant	0.03
sodium styrene sulfonate	co-monomer	0.18
B504-MA	polymerizable fluorescent dye	0.03

Supporting Information

Supporting Information is available from the Wiley Online Library or from the author.

Acknowledgements

We gratefully acknowledge Prof. Burkhard Dünweg for calculating the charge distribution of elongated particles, and Dr. Hans-Josef Beauvisage for helping us to calculate the mean curvature radius of an ellipsoid. Dr. Martin Dass and Andreas Hanewald are acknowledged for helping with electron microscopy and tensile testing. We also thank Sandra Seywald, Petra Räder, and Dr. Manfred Wagner for the GPC, thermogravimetric analysis, and NMR measurements, respectively.

[1] V. Mailänder, K. Landfester, *Biomacromolecules* **2009**, *10*, 2379.
[2] F. Zhao, Y. Zhao, Y. Liu, X. Chang, C. Chen, Y. Zhao, *Small* **2011**, *7*, 1322.
[3] A. Verma, F. Stellacci, *Small* **2010**, *6*, 12.
[4] S. Lorenz, C. P. Hauser, B. Autenrieth, C. K. Weiss, K. Landfester, V. Mailänder, *Macromol. Biosci.* **2010**, *10*, 1034.
[5] B. D. Chithrani, A. A. Ghazani, W. C. Chan, *Nano Lett.* **2006**, *6*, 662.
[6] J. A. Champion, Y. K. Katare, S. Mitragotri, *Proc. Natl. Acad. Sci. USA* **2006**, *103*, 4930.
[7] S. E. A. Gratton, P. A. Ropp, P. D. Pohlhaus, J. C. Luft, V. J. Madden, M. E. Napier, J. M. DeSimone, *Proc. Natl. Acad. Sci. USA* **2008**, *105*, 11613.
[8] X. Huang, X. Teng, D. Chen, F. Tang, J. He, *Biomaterials* **2010**, *31*, 438.
[9] S. Mitragotri, J. Lahann, *Nat. Mater.* **2009**, *8*, 15.
[10] P. Decuzzi, M. Ferrari, *Biomaterials* **2006**, *27*, 5307.
[11] P. Decuzzi, B. Godin, T. Tanaka, S. Y. Lee, C. Chiappini, X. Liu, M. Ferrari, *J. Control. Release* **2010**, *141*, 320.
[12] J. P. Rolland, B. W. Maynor, L. E. Euliss, A. E. Exner, G. M. Denison, J. M. DeSimone, *J. Am. Chem. Soc.* **2005**, *127*, 10096.
[13] J. H. Moon, A. J. Kim, J. C. Crocker, S. Yang, *Adv. Mater.* **2007**, *19*, 2508.
[14] F. Buyukserin, M. Aryal, J. M. Gao, W. C. Hu, *Small* **2009**, *5*, 1632.
[15] T. J. Merkel, K. P. Herlihy, J. Nunes, R. M. Orgel, J. P. Rolland, J. M. DeSimone, *Langmuir* **2010**, *26*, 13086.

[16] H. C. Shu, A. R. Bate, D. Lee, A. R. Studart, B. Wang, C.-H. Chen, J. Thiele, R. K. Shah, A. Krummel, D. A. Weitz, *Macromol. Rapid Commun.* **2010**, *31*, 108.
[17] C. C. Ho, A. Keller, J. A. Odell, R. H. Ottewill, *Colloid Polym. Sci.* **1993**, *271*, 469.
[18] K. M. Keville, E. I. Franses, J. M. Caruthers, *J. Colloid Interface Sci.* **1991**, *144*, 103.
[19] J. A. Champion, Y. K. Katare, S. Mitragotri, *Proc. Natl. Acad. Sci. USA* **2007**, *104*, 11901.
[20] B. Madivala, J. Fransaer, J. Vermant, *Langmuir* **2009**, *25*, 2718.
[21] B. Madivala, S. Vandebril, J. Fransaer, J. Vermant, *Soft Matter* **2009**, *5*, 1717.
[22] C. Herrmann, M. B. Bannwarth, K. Landfester, D. Crespy, *Macromol. Chem. Phys.* **2012**, *213*, 829.
[23] A. Mohraz, M. J. Solomon, *Langmuir* **2005**, *21*, 5298.
[24] Y. X. Hu, J. P. Ge, T. R. Zhang, Y. D. Yin, *Adv. Mater.* **2008**, *20*, 4599.
[25] A. C. Courbaron, O. J. Cayre, V. N. Paunov, *Chem. Commun.* **2007**, *6*, 628.
[26] D. Crespy, K. Landfester, *Beilstein J. Org. Chem.* **2010**, *6*, 1132.
[27] D. Crespy, K. Landfester, U. S. Schubert, A. Schiller, *Chem. Commun.* **2010**, *46*, 6651.
[28] A. Manzke, C. Pfahler, O. Dubbers, A. Plettl, P. Ziemann, D. Crespy, E. Schreiber, U. Ziener, K. Landfester, *Adv. Mater.* **2007**, *19*, 1337.
[29] M. Molberg, D. Crespy, P. Rupper, F. Nuesch, J. A. E. Manson, C. Lowe, D. M. Opris, *Adv. Funct. Mater.* **2010**, *20*, 3280.
[30] R. H. Staff, P. Rupper, I. Lieberwirth, K. Landfester, D. Crespy, *Soft Matter* **2011**, *7*, 10219–10226.
[31] J. Fickert, P. Rupper, R. Graf, K. Landfester, D. Crespy, *J. Mater. Chem.* **2012**, *22*, 2286–2291.
[32] D. Crespy, M. Stark, C. Hoffmann-Richter, U. Ziener, K. Landfester, *Macromolecules* **2007**, *40*, 3122.
[33] D. Crespy, K. Landfester, *Macromol. Chem. Phys.* **2007**, *208*, 457.
[34] D. Crespy, K. Landfester, *Polymer* **2009**, *50*, 1616.
[35] A. Musyanovych, J. Dausend, M. Dass, P. Walther, V. Mailänder, K. Landfester, *Acta Biomater.* **2011**, *7*, 4160–4168.
[36] V. Holzapfel, A. Musyanovych, K. Landfester, M. R. Lorenz, V. Mailänder, *Macromol. Chem. Phys.* **2005**, *206*, 2440.
[37] C. C. Ho, A. Keller, J. A. Odell, R. H. Ottewill, *Polym. Int.* **1993**, *30*, 207.
[38] C. C. Ho, M. J. Hill, J. A. Odell, *Polymer,* **1993**, *34*, 2019.
[39] E. Allémann, E. Doelker, R. Gurny, *Eur. J. Pharm. Biopharm.* **1993**, *39*, 13.
[40] M. J. Garvey, Th. F. Tadros, B. Vincent, *J. Colloid Interface Sci.* **1976**, *55*, 440.
[41] The experiments were repeated 2 times under the same conditions (n = 2), which are 20 h incubation, 75 μg mL^{-1}, and 150 μg mL^{-1} (data plotted in Figure 4). Also, higher uptake of spherical treated versus original particles was confirmed in the concentration and time series, which means in total 4 experiments give evidence of it (n′ = 4).
[42] M. M. Arnida, A. Janat-Amsbury, C. M. Ray, H. Peterson, *Eur. J. Pharm. Biopharm.* **2011**, *77*, 417.
[43] Y. Qiu, Y. Liu, L. Wang, L. Xu, R. Bai, Y. Li, X. Wu, Y. Zhao, Y. Li, C. Chen, *Biomaterials* **2011**, *31*, 7606.
[44] H. Meng, S. Yang, Z. Li, T. Xia, J. Chen, Z. Ji, H. Zhang, X. Wang, S. Lin, C. Huang, Z. H. Zhou, J. I. Zink, A. E. Nel, *ACS Nano* **2011**, *5*, 4434.
[45] J. Rejman, *Biochem. J.* **2004**, *377*, 159.
[46] C. C. Ho, R. H. Ottewill, L. Yu, *Colloid Surf. A* **1998**, *141*, 29.
[47] G. V. Sherbet, M. S. Lakshmi, K. V. Rao, *Experimental Cell Research* **1972**, *70*, 113.
[48] I. Nikiforow, J. Adams, A. M. Konig, A. Langhoff, K. Pohl, A. Turshatov, D. Johannsmann, *Langmuir* **2010**, *26*, 13162.
[49] K. Friedemann, A. Turshatov, K. Landfester, D. Crespy, *Langmuir* **2011**, *27*, 7132.
[50] K. Koynov, G. Mihov, M. Mondeshki, C. Moon, H. W. Spiess, K. Muellen, H.-J. Butt, G. Floudas, *Biomacromolecules* **2007**, *8*, 1745.
[51] G. Schmidtke-Schrezenmeier, M. Urban, A. Musyanovych, V. Mailänder, M. Rojewski, N. Fekete, C. Menard, E. Deak, K. Tarte, V. Rasche, K. Landfester, H. Schrezenmeier, *Cytotherapy* **2011**, *13*, 962.

Received: September 26, 2011
Revised: January 9, 2012
Published online: April 23, 2012

